

Supplemental Data

Supplemental Results

Characterization of CCL17⁺ DCs

Detailed FACS analyses of peripheral LNs from *Ccl17*^{E/+}, *Ccl17*^{E/E}, *Ccl17*^{E/+}*ApoE*^{-/-} and *Ccl17*^{E/E}*ApoE*^{-/-} mice confirmed that CCL17 expression is restricted to a subset of MHC-II⁺ CD11c⁺CD11b⁺CD8α⁻CD115⁻F4/80⁻440c⁻PDCA-1⁻ DCs (data not shown) (1). This was also evident in bone marrow-derived DCs (BMDCs) generated from *Ccl17*^{E/+} or *Ccl17*^{E/E} mice, where EGFP-expression was not detectable in undifferentiated progenitor cells but acquired during differentiation (**Supplemental Figure 13A**, not shown). As compared to EGFP⁻ DCs, unstimulated EGFP⁺*Ccl17*^{E/+} and EGFP⁺*Ccl17*^{E/E} DCs displayed higher surface expression of MHC-II (1) and of the co-stimulatory molecules CD40, CD80 and CD86, which was further enhanced by stimulation with TNF-α or LPS (**Supplemental Figure 13B**). In addition, EGFP⁺ *Ccl17*^{E/+} and *Ccl17*^{E/E} DCs revealed higher *Ccr7* transcript levels than EGFP⁻ DCs (data not shown). Notably, sorted EGFP⁻*Ccl17*^{E/+} DCs partially converted into CCL17-expressing EGFP⁺ DCs upon further culture over 1 day, likely reflecting their differentiation, whereas EGFP⁺ DCs did not convert back to EGFP⁻ DCs (**Supplemental Figure 13C**). As monocyte-derived TNF/iNOS-producing (Tip) DCs (2), similar to CCL17⁺ DCs, express high levels of co-stimulatory molecules and MHC-II, we addressed a phenotypic overlap of CCL17⁺ DCs and these cells. For analysis of Tip-DCs, BMDC were generated from BM as described (3). However, CCL17⁺ BMDCs did not express TNF in response to heat-killed *Listeria monocytogenes* or LPS, and cannot be stained with RB6-8C5 binding Ly6C/G (**Supplemental Figure 14A,B**), features characterizing Tip-DCs (2). Conversely, CCL17⁺ DCs express DEC205 (1), a marker absent on Tip-DCs (2). Thus, CCL17⁺ DCs represent a distinct, phenotypically mature DC subset.

Role of CCR4 in inflammatory recruitment and T-cell distribution

In an air-pouch model, recombinant mouse CCL17 dose- and time-dependently enhanced the inflammatory recruitment of CD4⁺ T cells and Tregs in vivo, compared to PBS-injected controls (**Figure 3C, Supplementary Figure 15**). When analyzing CD4⁺Foxp3⁺CD25⁺ Tregs among CD4⁺ T cells, however, we could not find a preferential role of CCL17 in the recruitment of Tregs (data not shown). A trend towards decreased CD4⁺ T cell and Treg numbers in the air pouch of *Ccr4*^{-/-} mice (**Supplementary Figure 15**) suggests a minor or partial role of CCR4 in CCL17-induced recruitment of CD4⁺ T cells.

Assessing the effect of CCR4 on T-cell distribution, we did not observe differences in CD4⁺ T-cell or Treg frequencies between *Ccr4*^{-/-} vs *Ccr4*^{+/+} mice (**Supplemental Figure 16A**). Moreover and in contrast to effects of CCL17 deficiency, we did not find differences in the frequencies of injected *Ccr4*^{-/-} CD4⁺ T cells or in expanded or converted *Ccr4*^{-/-} Tregs, when compared to wild-type counterparts after transfer into wild-type mice, or conversely, in the number of injected wild-type CD4⁺ T cells or Tregs after transfer into *Ccr4*^{-/-} vs *Ccr4*^{+/+} mice (**Supplemental Figure 16B,C**).

Functions of CCL17⁺ DCs in T-cell proliferation

We further assessed antigen-specific interactions of CCL17⁺ DCs and T cells in vivo, as well as the proliferation of aortic T cells. The antigen-specific proliferation of CFSE-labeled OVA-specific OT-II CD4⁺ T cells exposed to OVA-2-pulsed EGFP⁺*Ccl17*^{E/E} BMDCs or DCs sorted from peripheral LNs in vivo was increased, when compared to EGFP⁺*Ccl17*^{E/+} DCs (**Supplemental Figure 17A,B**). While addition of CCL17 to co-cultures of EGFP⁺*Ccl17*^{E/E} DCs and T cells reduced antigen-specific T-cell proliferation, an antibody to CCL17 increased T-cell proliferation in co-culture with *Ccl17*^{E/+} DCs (**Supplemental Figure 17C**).

We further evaluated effects on Treg and CD4⁺ T-cell proliferation within the aorta in short-term BrdU pulse-chase experiments. Flow cytometric analysis of aortic cell suspensions

2 hours after BrdU injection, however, revealed only few proliferating CD4⁺ T cells but no differences between atherosclerotic *Ccl17^{+/+}Apoe^{-/-}* and *Ccl17^{E/E}Apoe^{-/-}* mice (4.6±1.1% vs 3.6±1.2% BrdU⁺CD4⁺, n.s., n=5 each), whereas numbers of proliferating Tregs were below the detection limit.

Supplemental References

1. Alferink, J., Lieberam, I., Reindl, W., Behrens, A., Weiss, S., Huser, N., Gerauer, K., Ross, R., Reske-Kunz, A.B., Ahmad-Nejad, P., et al. Compartmentalized production of CCL17 in vivo: strong inducibility in peripheral dendritic cells contrasts selective absence from the spleen. *J Exp Med.* 2003;197(5):585-599.
2. Serbina, N.V., Salazar-Mather, T.P., Biron, C.A., Kuziel, W.A., and Pamer, E.G. TNF/iNOS-producing dendritic cells mediate innate immune defense against bacterial infection. *Immunity.* 2003;19(1):59-70.
3. Lutz, M.B., Kukutsch, N., Ogilvie, A.L., Rossner, S., Koch, F., Romani, N., and Schuler, G. An advanced culture method for generating large quantities of highly pure dendritic cells from mouse bone marrow. *J Immunol Methods.* 1999;223(1):77-92.

Supplemental Table 1

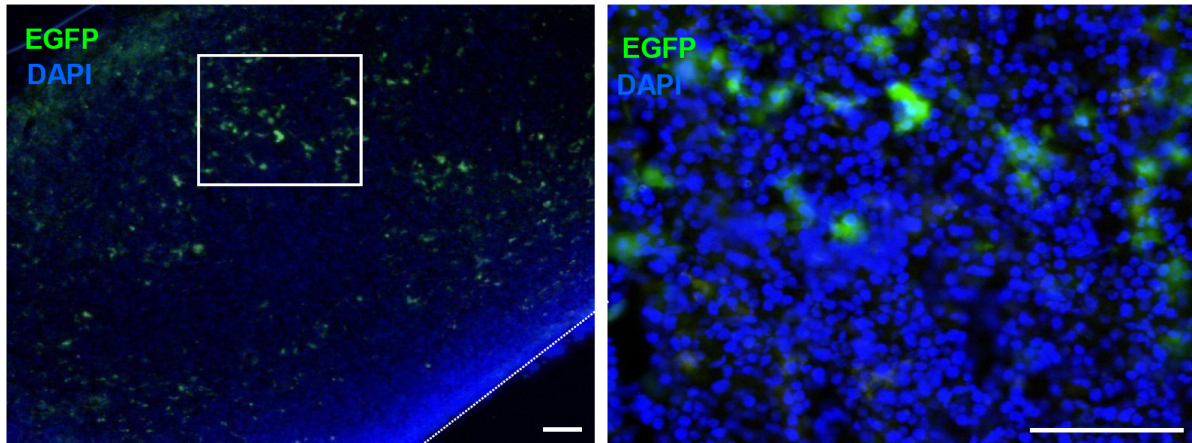
Serum lipid levels

Genotypes, disease model	total cholesterol (mg/dL)	LDL (mg/dL)	HDL (mg/dL)	triglycerides (mg/dL)
6 months normal chow				
<i>Ccl17</i> ^{+/+} <i>Apoe</i> ^{-/-}	353.7 ± 31.6	226.8 ± 21.3	140.8 ± 16.3	87.4 ± 10.1
<i>Ccl17</i> ^{E/E} <i>Apoe</i> ^{-/-}	386.5 ± 30.7	256.0 ± 24.9	172.5 ± 21.6	83.5 ± 13.9
High-fat diet, 12 weeks				
<i>Ccl17</i> ^{+/+} <i>Apoe</i> ^{-/-}	839.3 ± 67.2	558.0 ± 41.8	338.4 ± 11.3	213.9 ± 91.7
<i>Ccl17</i> ^{E/E} <i>Apoe</i> ^{-/-}	621.0 ± 51.2	487.0 ± 37.6	273.0 ± 30.7	100.4 ± 17.0
High-fat diet, 24 weeks				
<i>Apoe</i> ^{-/-} <i>Ccl17</i> ^{+/+} → <i>Apoe</i> ^{-/-}	600.1 ± 61.0	410.8 ± 35.1	125.2 ± 21.4	103.6 ± 17.6
<i>Apoe</i> ^{-/-} <i>Ccl17</i> ^{E/E} → <i>Apoe</i> ^{-/-}	662.3 ± 28.8	417.1 ± 14.9	128.9 ± 14.6	98.7 ± 11.2
Undepleted controls				
<i>Ccl17</i> ^{+/+} <i>Apoe</i> ^{-/-}	789.0 ± 31.0	553.5 ± 29.7	108.5 ± 2.5	117.2 ± 22.5
<i>Ccl17</i> ^{E/E} <i>Apoe</i> ^{-/-}	966.6 ± 9.6	656.7 ± 20.0	106.0 ± 4.9	130.3 ± 15.9
<i>Ccl17</i> ^{+/+} <i>Apoe</i> ^{-/-} mice transferred with CD4 ⁺ T cells (<i>Ccl17</i> ^{+/+} <i>Apoe</i> ^{-/-} donor)	725.5 ± 20.4	515.3 ± 18.4	102.5 ± 3.7	90.8 ± 5.7
CD4 ⁺ T cells (<i>Ccl17</i> ^{E/E} <i>Apoe</i> ^{-/-} donor)	681.0 ± 36.2	417.3 ± 29.3	95.0 ± 3.1	111.5 ± 14.5
<i>Ccl17</i> ^{E/E} <i>Apoe</i> ^{-/-} mice transferred with CD4 ⁺ T cells (<i>Ccl17</i> ^{+/+} <i>Apoe</i> ^{-/-} donor)	915.3 ± 53.3	590.3 ± 57.8	105.0 ± 4.5	125.8 ± 18.7
CD4 ⁺ T cells (<i>Ccl17</i> ^{E/E} <i>Apoe</i> ^{-/-} donor)	746.5 ± 71.9	517.2 ± 21.3	100.5 ± 1.6	127.3 ± 31.6
High-fat diet, 4 weeks				
<i>Ccl17</i> ^{+/+} <i>Apoe</i> ^{-/-} , isotype	740.8 ± 88.4	447.3 ± 33.0	104.3 ± 2.7	91.8 ± 12.9
<i>Ccl17</i> ^{E/E} <i>Apoe</i> ^{-/-} isotype	694.6 ± 21.4	446.8 ± 12.0	103.2 ± 2.4	82.8 ± 14.2
<i>Ccl17</i> ^{+/+} <i>Apoe</i> ^{-/-} , anti-CD25	535.6 ± 48.3	370.2 ± 41.5	88.0 ± 3.3	83.0 ± 8.0
<i>Ccl17</i> ^{E/E} <i>Apoe</i> ^{-/-} anti-CD25	667.3 ± 94.3	429.3 ± 54.7	105.3 ± 4.2	87.0 ± 8.2
High-fat diet, 12 weeks				
<i>Apoe</i> ^{-/-} → <i>Apoe</i> ^{-/-}	585.4 ± 62.9	452.4 ± 45.1	190.4 ± 30.0	75.0 ± 8.9
<i>Apoe</i> ^{-/-} → <i>Apoe</i> ^{-/-} <i>Ccl17</i> ^{E/E}	788.0 ± 65.7	610.0 ± 65.7	222.4 ± 64.2	100.4 ± 14.3
High-fat diet, 8 weeks				
isotype control	805.2 ± 95.6	643.6 ± 75.3	326.4 ± 40.2	64.2 ± 4.8
anti-CCL17	707.6 ± 32.2	557.4 ± 21.0	277.2 ± 15.5	60.4 ± 6.3

LDL, low-density lipoprotein
HDL, high-density lipoprotein

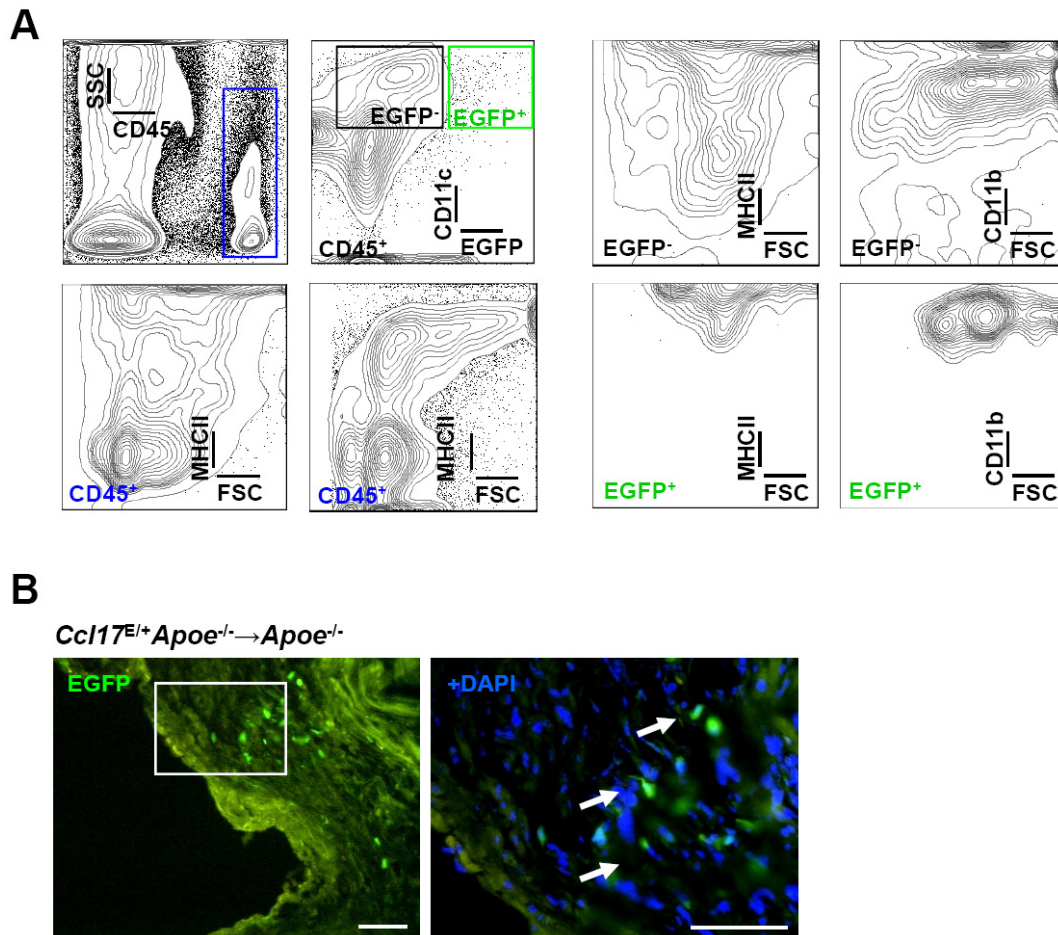
Supplemental Figures und Figure Legends

Ccl17^{E/+}Apoe^{-/-}



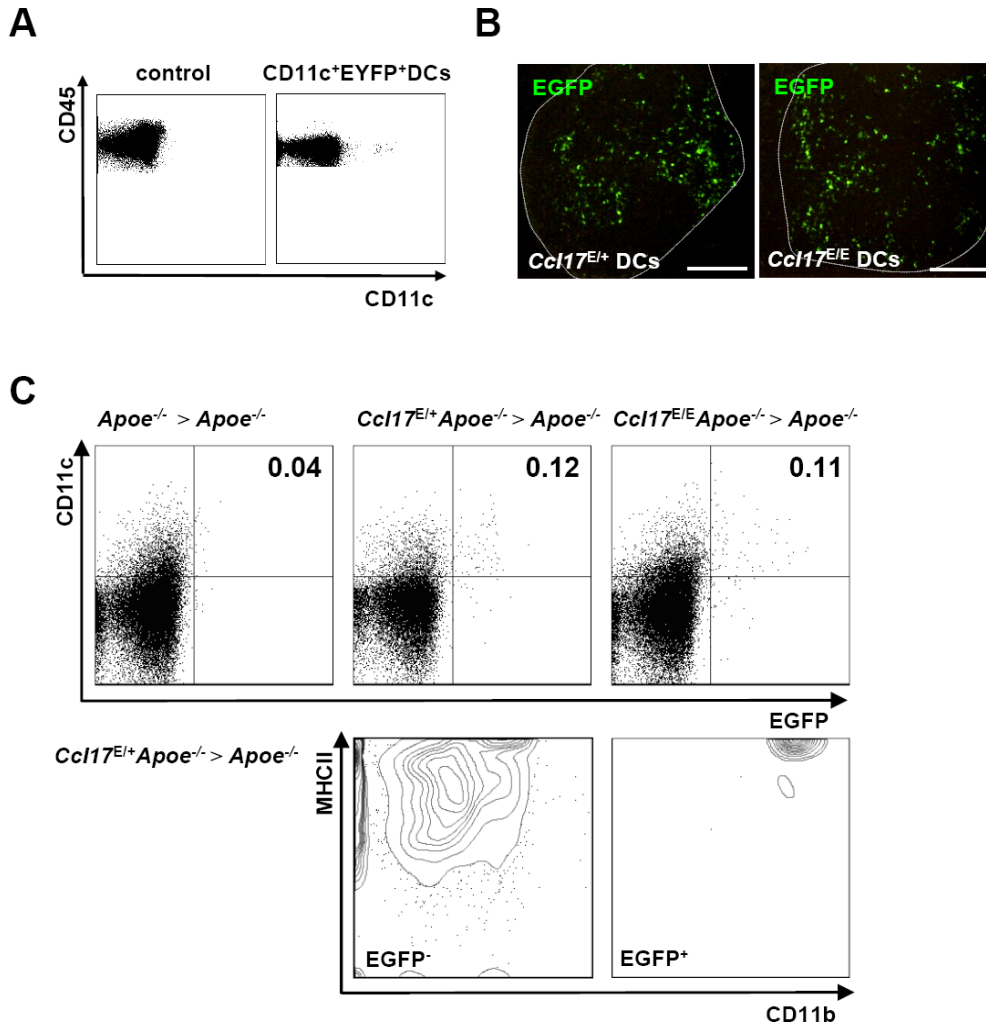
Supplemental Figure 1

EGFP⁺ DCs (green) can be frequently detected in perifollicular regions of LNs in naïve *Ccl17^{+E}Apoe^{-/-}* mice, as assessed by immunofluorescence microscopy; cell nuclei were counter-stained by DAPI (blue). Scale bars, 50 μ m.



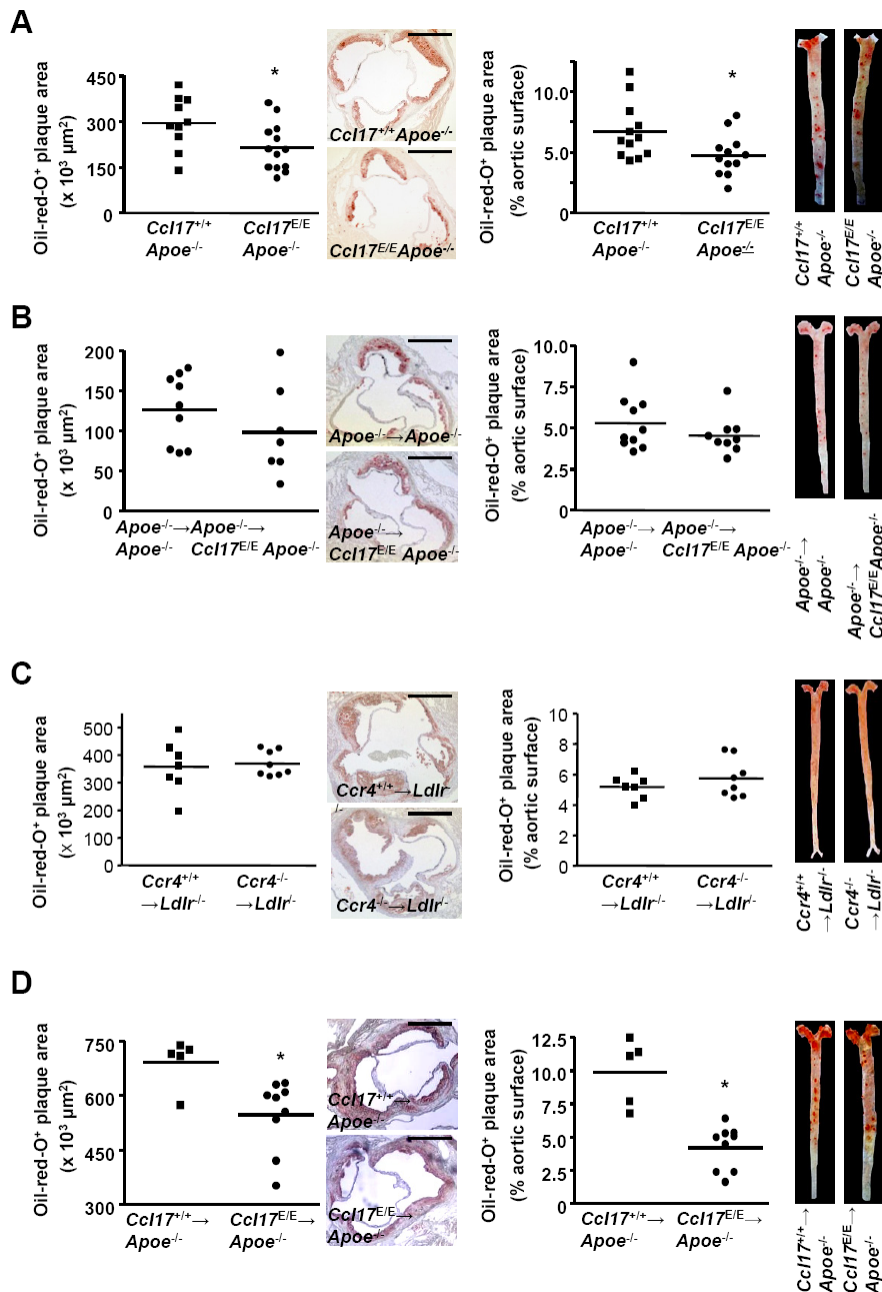
Supplemental Figure 2

(A) Flow cytometry of aortic cell suspensions was performed to analyze expression of CD11b and MHC-II in EGFP⁻CD11c⁺ DCs vs EGFP⁺CD11c⁺ aortic DCs from atherosclerotic *Ccl17^{E/+}Apoe^{-/-}* mice. (B) EGFP⁺ DCs accumulate in the atherosclerotic lesion of the aortic root and in the adventitia in chimeric *Ccl17^{E/+}Apoe^{-/-} → Apoe^{-/-}* mice 12 weeks after BM reconstitution and initiating a high-fat diet, as assessed by immunofluorescence microscopy; cell nuclei were counter-stained by DAPI (blue). Scale bars, 50 μ m.



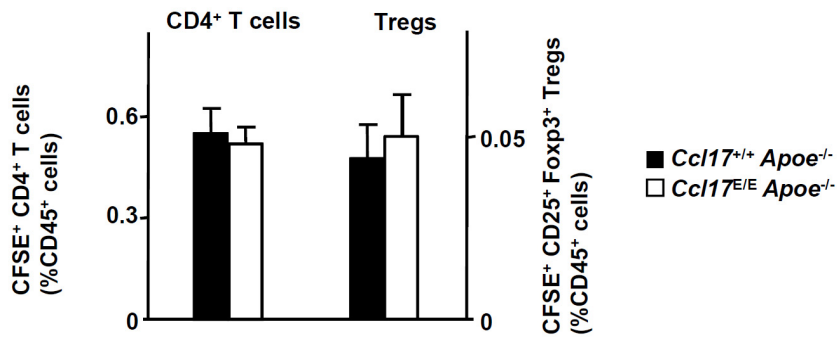
Supplemental Figure 3

(A) EYFP⁺CD11c⁺ DCs sorted from digested aortas of naïve CD11c-EYFP-mice were injected into the footpad of *Apoe*^{-/-} mice. After 18 hours, the presence of EYFP⁺ cells was analyzed in popliteal LNs by FACS analysis; representative dot plots are shown. (B) EGFP⁺ *Ccl17*^{E/+} or EGFP⁺ *Ccl17*^{E/E} BMDCs (green) in popliteal LNs of *Apoe*^{-/-} mice 18 hours after footpad injection; representative images are shown. Scale bars, 200 μ m. (C) FACS analysis of CD11c⁺ EGFP⁺ DCs in paraaortic LNs of *Apoe*^{-/-} mice 4 weeks after orthotopic transplantation of an infrarenal aorta from *Ccl17*^{+/+}*Apoe*^{-/-}, *Ccl17*^{E/+}*Apoe*^{-/-} or *Ccl17*^{E/E}*Apoe*^{-/-} mice (upper panels). EGFP⁻CD11c⁺ and EGFP⁺CD11c⁺ DCs were further analyzed for expression of MHC-II and CD11b (lower panels). Representative dot plots of n=3 mice per group are shown.



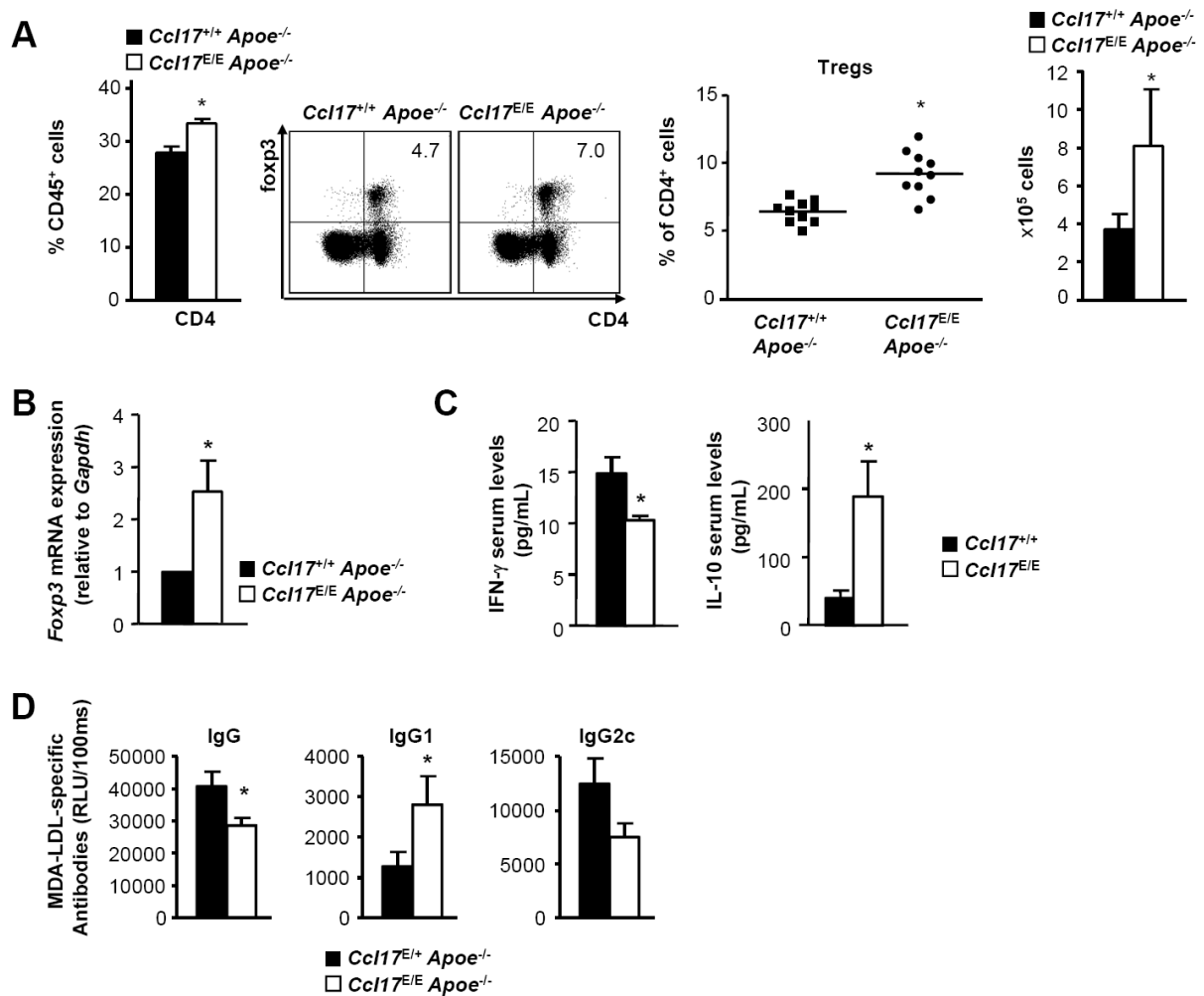
Supplemental Figure 4

(A) Atherosclerotic lesions were quantified in the aortic root and thoracoabdominal aorta after staining with oil-red O in *Ccl17*^{+/+}*Apoe*^{-/-} and *Ccl17*^{E/E}*Apoe*^{-/-} mice receiving a high-fat diet for 12 weeks; representative images of the aortic root and the thoracoabdominal aorta are shown. (B) *Ccl17*^{+/+}*Apoe*^{-/-} or *Ccl17*^{E/E}*Apoe*^{-/-} mice were transplanted with *Apoe*^{-/-} BM (*Apoe*^{-/-} → *Apoe*^{-/-} or *Apoe*^{-/-} → *Ccl17*^{E/E}). After 12 weeks of high-fat diet, atherosclerotic lesions were quantified in the aortic root and thoracoabdominal aorta after staining with oil-red-O; representative images are shown. (C) *Ldlr*^{-/-} mice were transplanted with *Ccr4*^{+/+} or *Ccr4*^{-/-} BM (*Ccr4*^{+/+} → *Ldlr*^{-/-} or *Ccr4*^{-/-} → *Ldlr*^{-/-}). After 12 weeks of high-fat diet, atherosclerotic lesions were quantified in the aortic root and thoracoabdominal aorta after staining with oil-red-O; representative images are shown. (D) *Apoe*^{-/-} mice fed a high-fat diet for 12 weeks were transplanted with either *Ccl17*^{+/+}*Apoe*^{-/-} (*Ccl17*^{+/+} → *Apoe*^{-/-}) or *Ccl17*^{E/E}*Apoe*^{-/-} BM (*Ccl17*^{E/E} → *Apoe*^{-/-}). After an additional 12 weeks of high-fat diet, atherosclerotic lesions were quantified in the aortic root and thoracoabdominal aorta after staining with oil-red O; representative images are shown. Data points represent frequencies of cells in individual mice, horizontal bars denote mean of all mice. Scale bars, 500 μm. **P*<0.05.



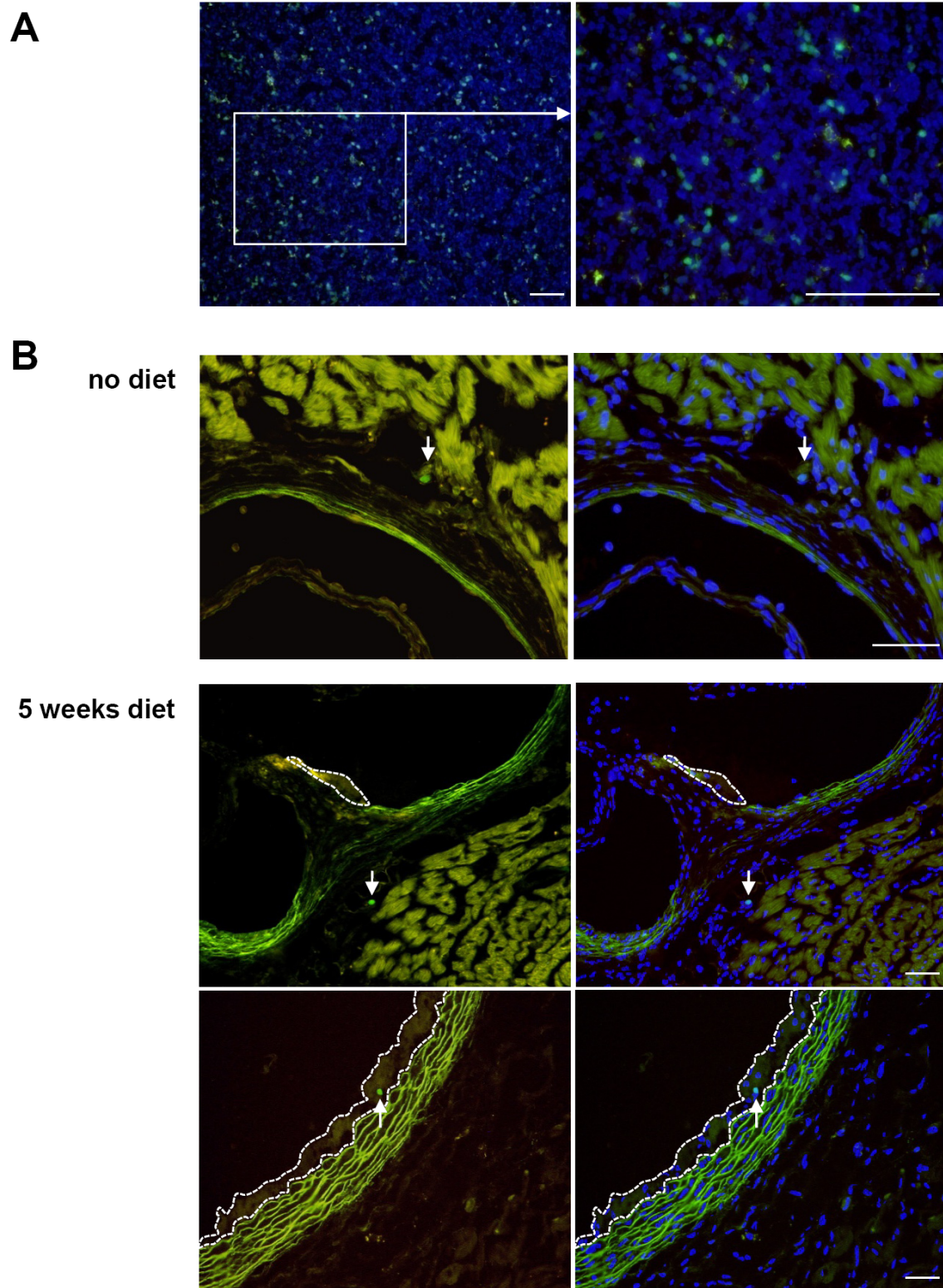
Supplemental Figure 5

CFSE⁺CD4⁺T cells were transferred into *Ccl17^{+/+}* or *Ccl17^{E/E}* mice. After 2h, homing of CFSE⁺CD4⁺T cells and CFSE⁺CD4⁺Foxp3⁺CD25⁺ Tregs to peripheral LN was quantified by FACS analysis (n=5).



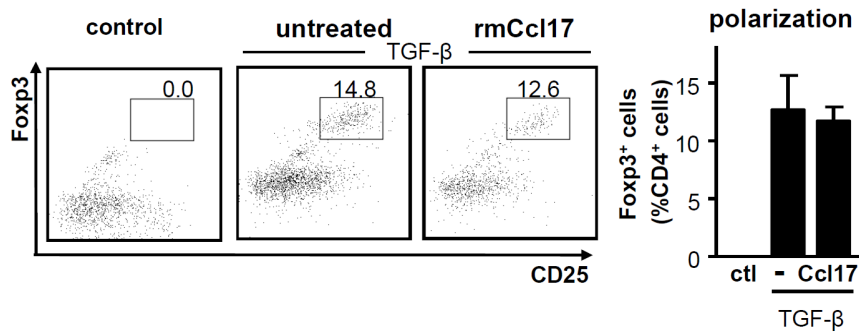
Supplemental Figure 6

(A) Flow cytometric analysis of CD3⁺CD4⁺ T cells and CD4⁺Foxp3⁺CD25⁺ Tregs and absolute numbers of Tregs in LNs of *Ccl17*^{+/+}*Apoe*^{-/-} and *Ccl17*^{E/E}*Apoe*^{-/-} mice employing indicated surface markers. Representative dot plots are shown; inserted numbers indicate percentages of CD4⁺ events. Data points represent frequencies of cells in individual mice, horizontal bars denote mean of all mice. (B) Real-time PCR analysis of *Foxp3* mRNA expression in LN of *Ccl17*^{+/+}*Apoe*^{-/-} and *Ccl17*^{E/E}*Apoe*^{-/-} mice. (C) Ifn- γ and IL-10 protein levels in serum of *Ccl17*^{+/+} and *Ccl17*^{E/E} mice. (n=8). (D) Specific IgG, IgG1 and IgG2c antibody titers to MDA-LDL were determined in the serum of 6 months old *Ccl17*^{+/E}*Apoe*^{-/-} and *Ccl17*^{E/E}*Apoe*^{-/-} mice by ELISA. Data are presented as relative light units (RLU) / 100 ms. **P*<0.05.



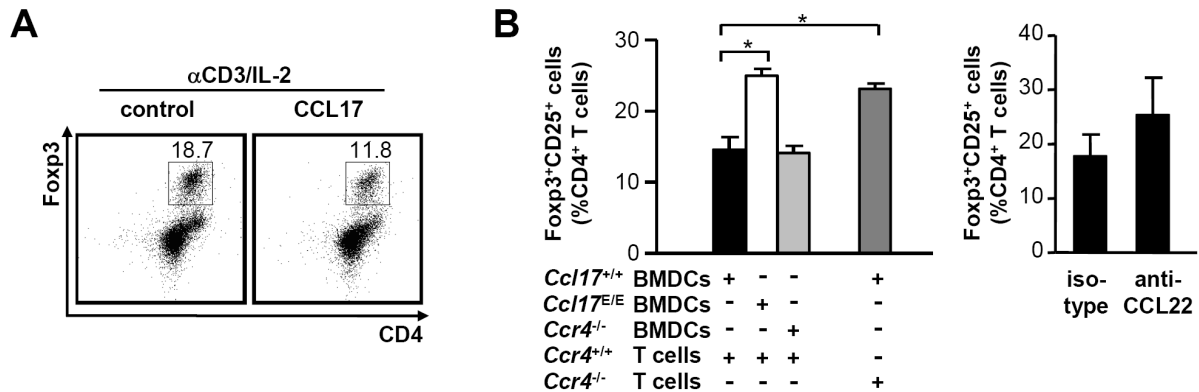
Supplemental Figure 7

(A) Foxp3⁺ (GFP⁺) cells can be detected in LNs of *Ldlr*^{-/-} mice reconstituted with *Foxp3gfp.KI* BM and (B) in the adventitia of mice before diet (upper panels) and during lesion formation, as well as in early plaques in the aortic root (lower panels) of these mice after 5 weeks of high-fat diet; cell nuclei were counter-stained by DAPI (blue). Plaques are demarcated by dashed lines. Scale bars, 50 μ m.



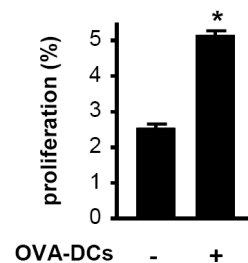
Supplemental Figure 8

CD4⁺ T cells were cultured under Treg polarization conditions in the presence of TGF-β with and without addition of recombinant mouse rmCCL17. Frequencies of Foxp3⁺CD25⁺ Tregs among CD4⁺ T cells were analyzed by flow cytometry. Representative dot plots and percentages within quadrants are shown (n=5).



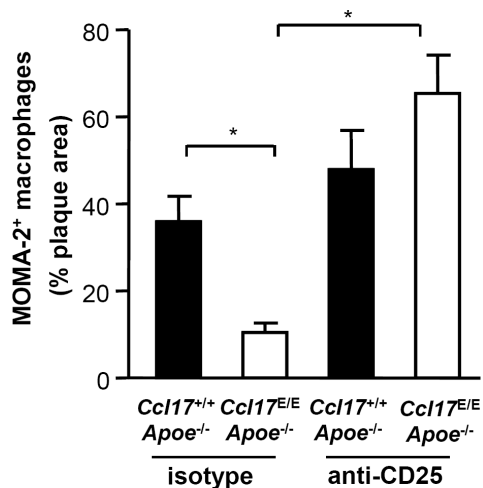
Supplemental Figure 9

(A) Tregs were re-stimulated with anti-CD3/IL-2 in the absence or presence of CCL17 for 2 days. Frequencies of Foxp3⁺CD25⁺ Tregs among CD4⁺ T cells were analyzed by FACS. Representative dot plots are shown; inserted numbers indicate percentages of CD4⁺ events. (B) *Ccl17*^{+/+}, *Ccl17*^{E/E} or *Ccr4*^{-/-} BMDCs were incubated with Tregs differentiated from wild-type or *Ccr4*^{-/-} T cells (left panel) and BMDCs were incubated with Tregs in the presence of IgG isotype control or anti-CCL22 antibody (5 μg/mL, right panel, n=3-8). Frequencies of Foxp3⁺CD25⁺CD4⁺ Tregs among CD4⁺ cells were quantified by FACS analysis after 3 days. **P*<0.05.



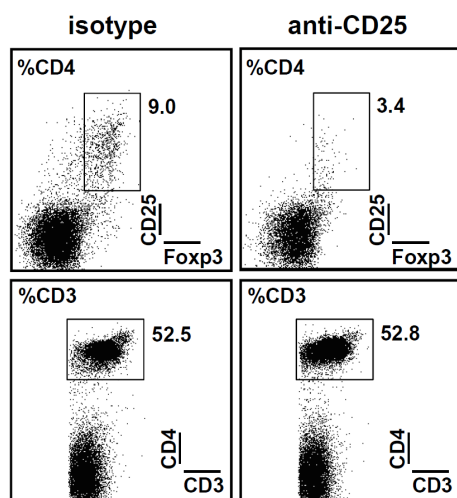
Supplemental Figure 10

EYFP⁺CD11c⁺ DCs sorted from digested aortas of naïve CD11c-EYFP-mice were loaded with OVA and incubated with OT-II CD4⁺ T cells; T-cell proliferation was quantified by CFSE dilution and FACS analysis after 3 days. n=3. **P*<0.05.



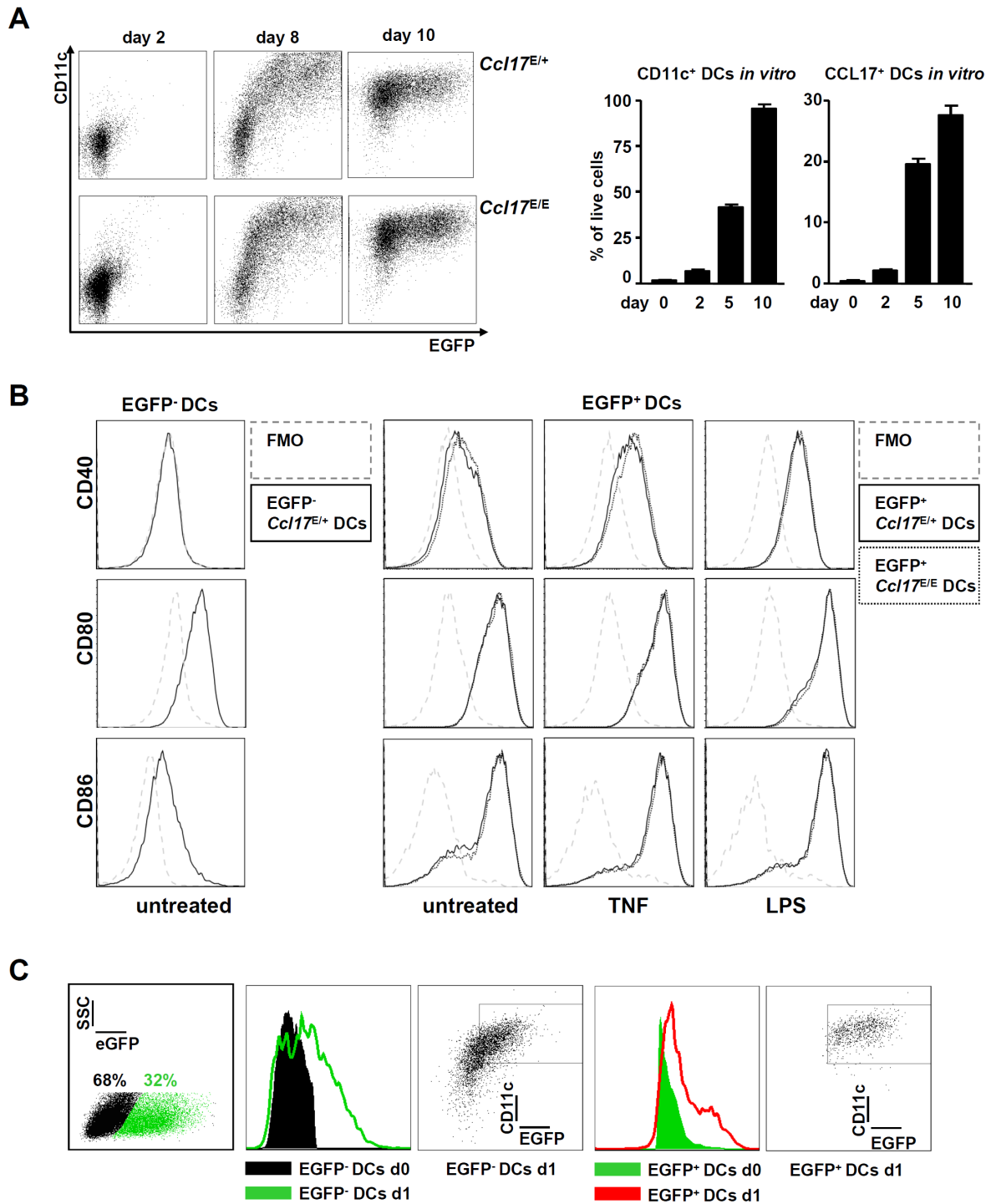
Supplemental Figure 11

The relative content of MOMA-2⁺ macrophages per plaque area was analyzed by quantitative immunofluorescence in *Ccl17*^{+/+} *ApoE*^{-/-} and *Ccl17*^{E/E} *ApoE*^{-/-} mice treated with depleting anti-CD25 antibody or isotype control and fed a high-fat diet for 4 weeks. **P*<0.05.



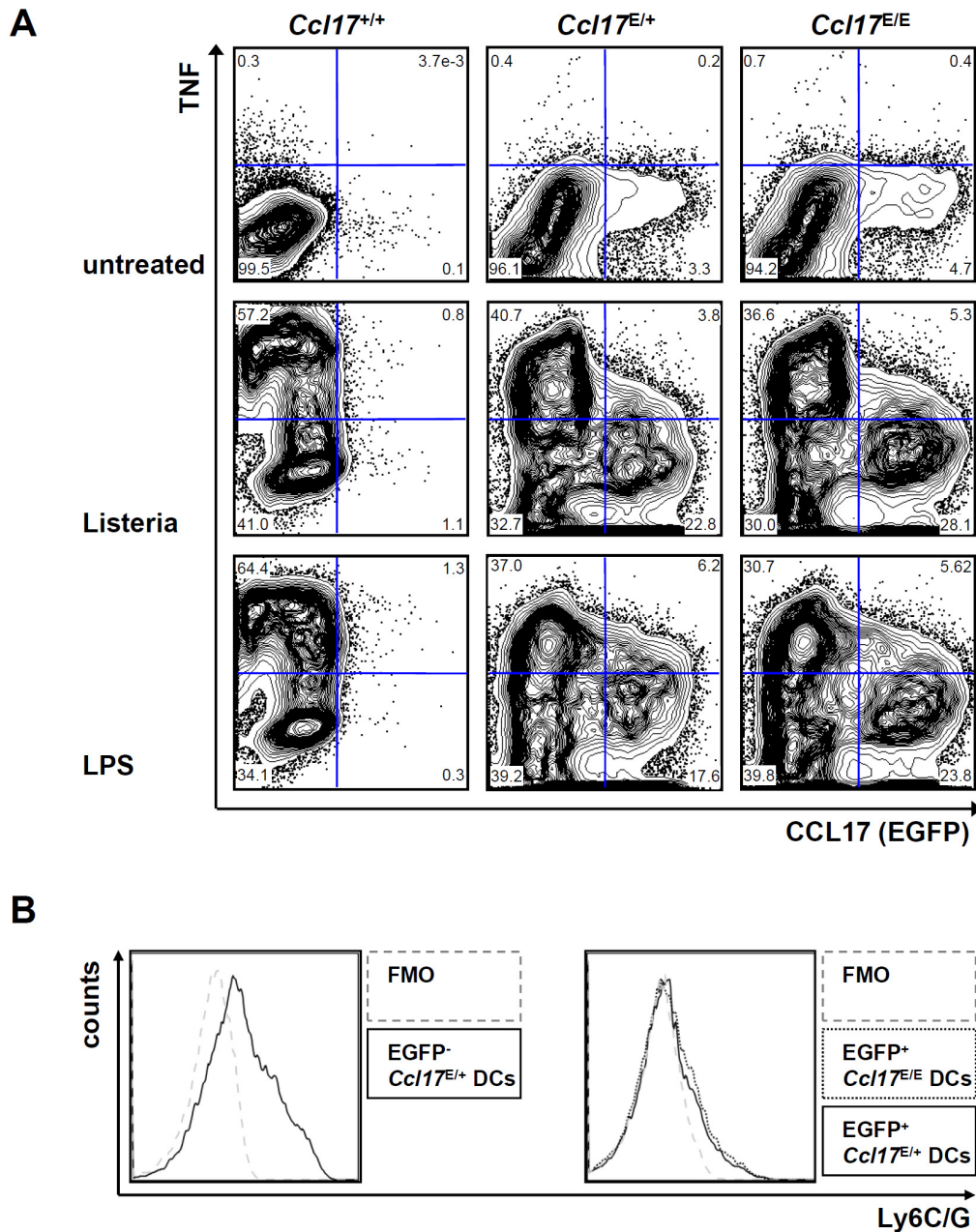
Supplemental Figure 12

One week after injection with a depleting anti-CD25 antibody, frequencies of CD25⁺Foxp3⁺ Tregs among CD4⁺ T cells and CD4⁺ T cells among CD3⁺ T cells were analyzed by flow cytometry; representative dot plots are shown.



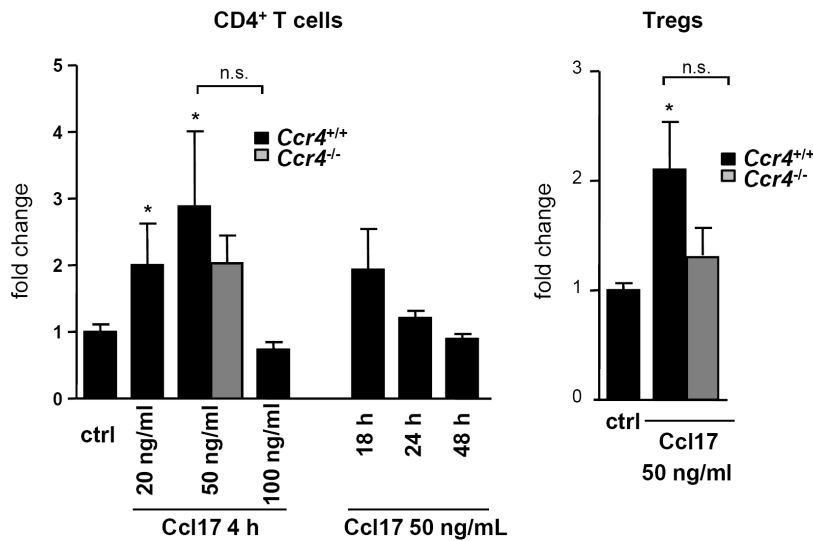
Supplemental Figure 13

(A) DCs were differentiated from Flt3⁺ progenitor cells generated from BM of *Ccl17^{E/+}* or *Ccl17^{E/E}* mice. EGFP and CD11c expression were assessed at indicated time points by FACS analysis; representative dot plots are shown. Quantification of the frequencies of CD11c⁺ and CD11c⁺CCL17⁺ DCs among cells generated from *Ccl17^{E/+}* BM at the time points indicated (n=3). (B) The expression of co-stimulatory molecules was assessed in untreated and overnight TNF (50 ng/mL) or LPS (1 μ g/ml)-treated EGFP⁻*Ccl17^{E/+}*, EGFP⁺*Ccl17^{E/+}* and EGFP⁺*Ccl17^{E/E}* BMDCs by FACS analysis; representative histograms are shown, dashed lines indicate controls (FMO/fluorescence minus one). (C) EGFP⁻ and EGFP⁺*Ccl17^{E/+}* BMDCs were sorted (day 0) and EGFP and CD11c expression were assessed by FACS analysis at indicated time points; representative histograms and dot plots are shown.



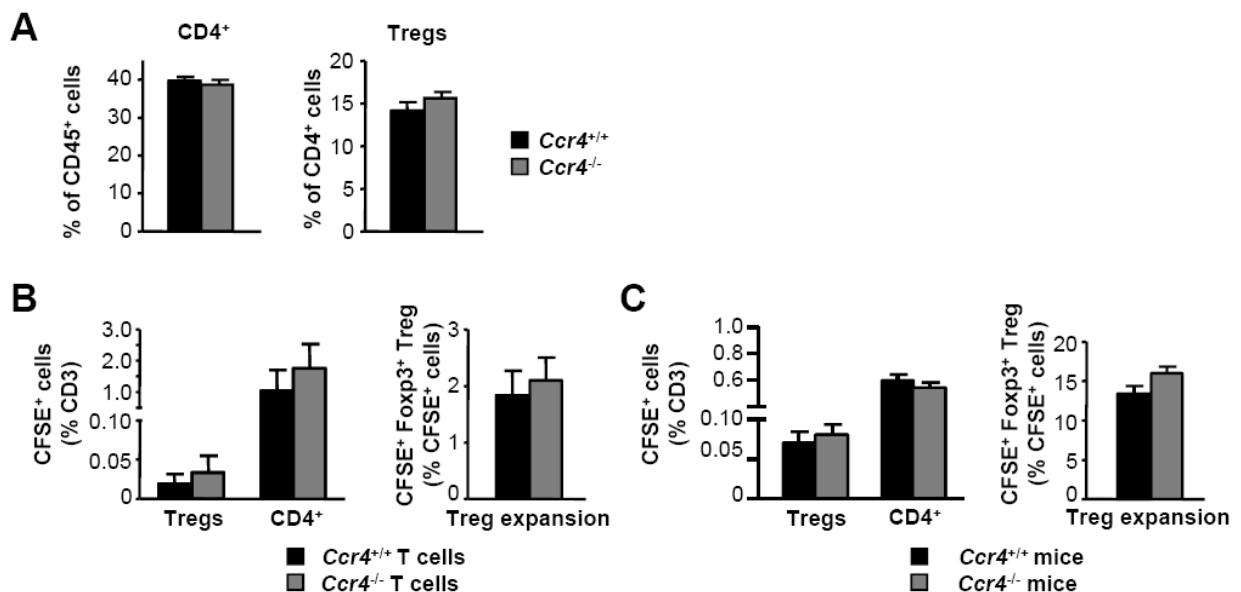
Supplemental Figure 14

(A) DCs were differentiated from BM of *Ccl17*^{+/+}, *Ccl17*^{E/+} or *Ccl17*^{E/E} mice. Intracellular TNF- α expression and EGFP expression was analyzed in untreated DCs, and overnight heat-killed *Listeria monocytogenes* (50 μ g/mL,) or LPS (1 μ g/mL)-treated DCs by FACS analysis; representative dot blots are shown. (B) Ly6C/G expression was analyzed in EGFP⁻ and EGFP⁺ *Ccl17*^{E/+} BMDCs by FACS analysis; representative histograms are shown, dashed lines indicate controls (FMO/fluorescence minus one).



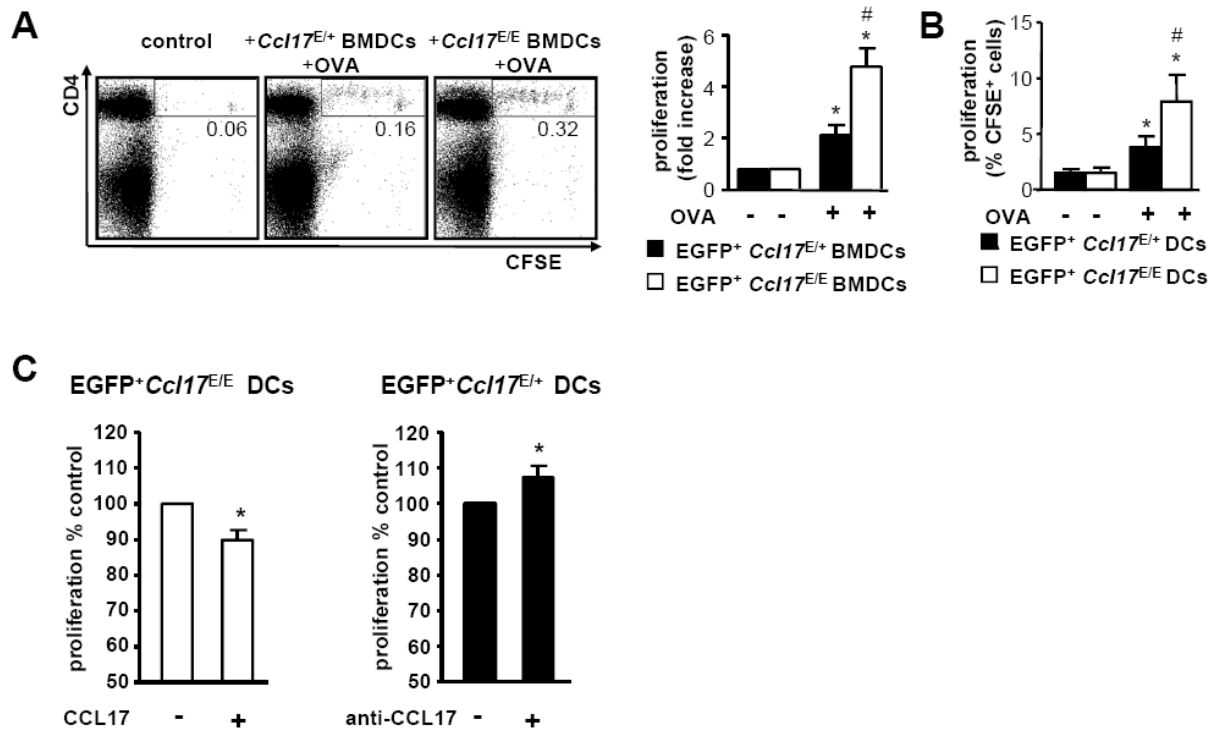
Supplemental Figure 15

Recruitment of CD4⁺ T cells and CD4⁺Foxp3⁺CD25⁺ Tregs into air pouches of wild-type or *Ccr4*^{-/-} mice in response to PBS (control) or recombinant mouse CCL17 (at indicated concentrations) was determined by quantifying absolute numbers of migrated cells in lavage fluid after time points indicated. Bars represent mean±SEM, normalized to control (n=3-8 mice each). **P*<0.05 vs control.



Supplemental Figure 16

(A) Flow cytometric analysis of CD3⁺CD4⁺ T cells and CD4⁺Foxp3⁺CD25⁺ Tregs in LNs of *Ccr4*^{+/+} and *Ccr4*^{-/-} mice employing indicated surface markers (n= 5 mice each). (B) CFSE-labeled *Ccr4*^{+/+} or *Ccr4*^{-/-} CD4⁺CD25⁻ T cells were transferred into wild type mice and frequencies of CFSE⁺Foxp3⁺ Tregs and CFSE⁺CD4⁺ cells among T cells in LNs were analyzed by flow cytometry after 10 days (n=5 per group). (C) CFSE-labeled CD4⁺CD25⁻ T cells were transferred into *Ccr4*^{+/+} or *Ccr4*^{-/-} mice and frequencies of CFSE⁺ Foxp3⁺ Tregs and CFSE⁺CD4⁺ cells among T cells in LNs were analyzed by flow cytometry after 10 days (n=5 per group).



Supplemental Figure 17

(A) Sorted EGFP⁺*Ccl17*^{E/+} BMDCs (unpulsed control), OVA-2-pulsed EGFP⁺*Ccl17*^{E/+} or EGFP⁺*Ccl17*^{E/E} BMDCs were transferred into wild-type mice transfused with CFSE⁺OT-II T cells. After 3 days, T-cell proliferation was quantified by CFSE dilution and FACS analysis; representative dot plots and percentage of CFSE⁺CD4⁺ T cells within gates are shown (n=6 independent experiments). **P*<0.05 vs unpulsed; #*P*<0.05 vs OVA-pulsed EGFP⁺*Ccl17*^{E/+} BMDCs. (B) EGFP⁺*Ccl17*^{E/+} or EGFP⁺*Ccl17*^{E/E} DCs (controls), OVA-2-pulsed EGFP⁺*Ccl17*^{E/+} or EGFP⁺*Ccl17*^{E/E} DCs sorted from LNs of *Ccl17*^{E/+} or *Ccl17*^{E/E} mice were transferred into wild-type mice transfused with CFSE⁺OT-II T cells. After 3 days, T-cell proliferation was quantified by CFSE dilution and FACS analysis (n=6). (C) Sorted OVA-2-pulsed EGFP⁺*Ccl17*^{E/+} or EGFP⁺*Ccl17*^{E/E} BMDCs (serving as controls for normalization) were incubated with OT-II T cells in the presence of a blocking antibody to CCL17 (10 μg/mL) or recombinant CCL17 (20 ng/mL). T-cell proliferation was quantified by CFSE dilution and FACS analysis after 3 days. **P*<0.05.

Supplemental Videos

Supplemental Video 1

Multiphoton microscopy of an *en face* prepared aorta of a CD11c-EYFP reporter mouse to visualize EYFP⁺CD11c⁺ DCs (green); collagen was visualized with second-harmonic generation (blue). A representative z-stack of a 30μm-thick volume is shown.

Supplemental Video 2

Multiphoton microscopy of an *en face* prepared aorta of a naïve wild-type mouse after immunostaining for MHC-II (red). A representative z-stack is shown.

Supplemental Video 3

Multiphoton microscopy of an *en face* prepared atherosclerotic aortic root of a *Ccl17^{E/+} ApoE^{-/-}* mouse on normal chow. A representative z-stack is showing EGFP⁺ DCs (bright green cytoplasmic staining, indicated by arrows). Nuclei are counter-stained with propidium iodide (PI). PI staining may appear yellow due to unspecific background fluorescence. Collagen is visible due to SHG (blue).